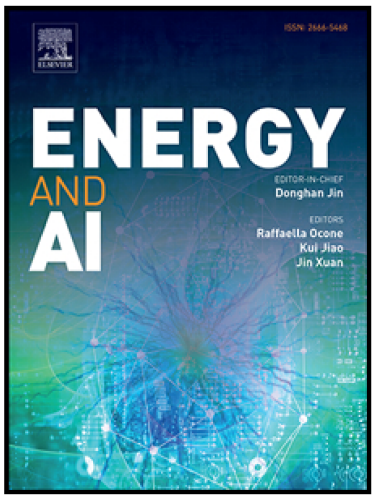

Screening Outstanding Mechanical Properties and Low Lattice Thermal Conductivity Using Global Attention Graph Neural Network

Joshua Ojih , Alejandro Rodriguez , Jianjun Hu , Ming Hu

PII: S2666-5468(23)00058-7
DOI: https://doi.org/10.1016/j.egyai.2023.100286
Reference: EGYAI 100286

To appear in: *Energy and AI*

Received date: 22 March 2023
Revised date: 19 May 2023
Accepted date: 24 June 2023

Please cite this article as: Joshua Ojih , Alejandro Rodriguez , Jianjun Hu , Ming Hu , Screening Outstanding Mechanical Properties and Low Lattice Thermal Conductivity Using Global Attention Graph Neural Network, *Energy and AI* (2023), doi: https://doi.org/10.1016/j.egyai.2023.100286

Highlights

- Global attention graph neural network model was trained for 5 mechanical properties.
- Mechanical properties of 775,947 structures from the million-scale open quantum material database were predicted in search of materials with ultrahigh hardness.
- 2 previously unreported super hard materials were identified.
- Bulk modulus was used for screening low lattice thermal conductivity materials.

Screening Outstanding Mechanical Properties and Low Lattice Thermal Conductivity Using Global Attention Graph Neural Network

Joshua Ojih[1], Alejandro Rodriguez[1], Jianjun Hu[2], Ming Hu[1,*]

[1]Department of Mechanical Engineering, University of South Carolina, SC 29208, USA

[2]Department of Computer Science and Engineering, University of South Carolina, SC 29208, USA

Abstract

Mechanical and thermal properties of materials are extremely important for various engineering and scientific fields such as energy conversion and energy storage. However, the characterization of these properties via high throughput screening at the quantum level, although highly accurate, is inefficient and very time- and resource-consuming. In contrast, prediction at the classical level is highly efficient but less accurate. We deploy scalable global attention graph neural network for accurate prediction of mechanical properties which bridge the gap between the accuracy at the quantum level and efficiency at the classical level. Using 10,158 elastic constants as training data, we trained the models on 5 mechanical properties, namely bulk modulus, shear modulus, Young's modulus, Poisson's ratio, and hardness. With the trained model, we predicted 775,947 data in search of materials with ultrahigh hardness. We further verify the recommended ultrahigh hardness materials by high precision first principles calculations, and we finally identify 20 structures with extreme hardness close to diamond, the hardest material in nature. Among those, two super hard materials are completely new and have not been reported in literature so far. We further recommend potential materials from bulk modulus prediction to search low lattice thermal conductivity, and we verify the thermal conductivity of 338 structures with first principles. Our results demonstrate that one can find materials with extreme mechanical properties recommended by graph neural network and low thermal conductivity material from bulk modulus prediction with minimal first principles calculations of the structures (only 0.04%) in the large-scale materials pool.

Keywords: Graph neural network, machine learning, mechanical properties, ultrahigh hardness, lattice thermal conductivity, DFT calculations, novel material discovery

* Author to whom all correspondence should be addressed. E-mail: hu@sc.edu (M.H.)

1. INRTODUCTION

The rapid development of industries has led to an increase in demand for steel and other materials for manufacturing. Choosing materials that can meet the desired properties is a key issue facing material scientists and engineers. One of the key components is understanding and cataloging the mechanical properties of materials for rapid testing and deployment in engineering applications[1], hence the need to calculate or predict these properties. For example, the ratio of bulk to shear modulus has been used as a basis to understand and predict the ductility of materials[2], whereby Pugh analysis have been used to derive descriptors for hardness in order to discover new hard materials[3]. Low lattice thermal conductivity (LTC) of crystalline materials is another desirable physical property in many applications, including but not limited to thermoelectric devices for waste heat recovery and energy conversion, thermal barrier coatings for that provide thermal protection in extremely high temperature environment, solid-solid phase change materials for solid state refrigeration and cooling, and energy storage[4]. LTC influences the efficiency of heat transfer and photon emission in energy generation technologies such as thermoelectric energy conversion, thermophotovoltaics devices[5]. However, the discovery of low LTC materials is a challenging task due to the complex interplay between various factors, such as atomic structures, chemical bonding, that determine the LTC. Although first-principles based anharmonic lattice dynamics is one of the most featured methods to obtain phonon properties[6–10] such method is impractical for high-throughput search of target thermal materials. From the domain knowledge, one of the governing factors is the bulk modulus, which measures the resistance of a material to compression and is closely related to the speed of sound, or broadly group velocities of phonons, in a crystal. Therefore, searching mechanical properties can also be beneficial for finding materials with desired LTC.

Historically, material scientists rely on either experiments or simulation for material characterization[11]. From theoretical point of view, numerical characterization of these properties at the quantum level is accurate and time consuming[12], while at the classical level it is efficient but less accurate[13,14]. Compromising the advantages of quantum mechanics calculations and classical modeling would be a good solution to quickly screen and predict materials properties. In recent years, machine learning (ML) and deep learning has been used for structure property prediction and been deployed in the field of material science in many different applications[15–20] such as superconductors[21], photovoltaics, thermoelectric, super hard materials[22–24]. Yufeng et al[25] has used *ab initio* calculations in investigating the elastic and mechanical properties of B19TiAl intermetallic compounds, and Han et al[26] used neural network based surrogate model to reduce the number of finite-element method conical indentation simulations to extract material properties. Though machine learning and deep learning is highly efficient, it has some limitations which reduces its accuracy in predicting properties. Such limitations include target measurement error[27], reliance on high-quality data[28], poor in extrapolation[29,30], and artifacting(noise)[31]. However, machine learning is now being used for the discovery of novel materials, its accuracy depends on the input representation of the crystal structures[18,24,32], and such representations are called descriptors or features. The scalable global attention graph neural network (deeperGATGNN)[33] model was used in this study for training the mechanical properties, which was developed by Sadman et al in 2021 based on previously global attention graph neural network (GATGNN)[15]. The deeperGATGNN model combines the descriptors and learning model into one step, and the model learns material properties directly from the connection of atoms in the crystals[34]. Thus, this model improves its accuracy in predicting material properties. In addition, the atomistic line graph neural network (ALIGNN)[35] was used to train the bulk modulus for the purpose of screening low LTC. In this study, we deploy scalable global attention graph neural network (deeperGATGNN) for accurate prediction of mechanical properties and the ALIGNN for accurate training and predicting bulk modulus as screening strategy for identifying materials with low lattice thermal conductivity, based on the prediction of the bulk modulus, thus bridging the gap between quantum level

accuracy and classical level efficiency leading to efficient screening and finding of novel materials. After screening 775,947 crystal structures from the million-scale open quantum material database (OQMD), we identified 20 structures with ultrahigh hardness and verified the LTC of 338 materials, among which 273 structures have LTC below 10 W/mK.

2. METHODOLOGY

Our approach was mainly training an ML model to predict mechanical properties on a pool of structures from OQMD[36,37]. Secondly, we used the prediction of bulk modulus to recommend low LTC materials.

2.1 Data generation and machine learning model

The 10,158 elastic constants training data are obtained from Jarvis-DFT database[38,39], with 70% of our data used for training and 30% for testing. Then, the model is deployed to predict inorganic crystal structures taken from OQMD database. Originally, there were about 1 million structures collected in the OQMD. After downloading these structures, we exclude the structures whose elements have never showed up in the training dataset. We finally ended up with 775,947 crystal structures for the screening pool. The deeperGATGNN was used in this work and has found success in material discovery for accurate and efficient prediction of material properties[18,40]. GATGNN uses two graph soft-attention variants to learn structural properties[41,42]. These attention layers are called augmented graph attention (AGAT) layers because they augment the node feature vectors with the features from connecting edge. Because these AGAT layers are only used to extract the locally dependent features, GATGNN then uses a unique soft-attention at the end to transform neighborhood-dependent information to global context. The soft attention $\alpha_{i,j}$ between a node i and a neighbor j can be represented as

$$\alpha_{i,j} = \frac{\exp(a_{i,j})}{\sum_{k \in N_i} \exp(a_{i,k})} \quad (1)$$

where N_i represents the neighborhood of node i and $a_{i,j}$ is the parameterized weight coefficients between nodes i and j which represents the importance of node j to node i. The global attention g_i, which is applied right before the global pooling, calculates each node's overall importance. It can be described as

$$g_i = \frac{(\boldsymbol{x_i} \,||\, \boldsymbol{E})\cdot \boldsymbol{W}}{\sum_{x_c \in \boldsymbol{X}} (\boldsymbol{X_c} \,||\, \boldsymbol{E})\cdot \boldsymbol{W}} \quad (2)$$

where $X \in \mathbb{R}^F$ represents a learned embedding, $\boldsymbol{E}$ is a compositional vector of the crystal, $\boldsymbol{W} \in \mathbb{R}^{1\times(F+|E|)}$ is a parameterized matrix, and $\boldsymbol{X_c}$ is the learned embedding of any atom c within the crystal. The main advantage of deeperGATGNN is the ability to perform with increasing graph convolutional (GC) layers. Our model was trained for a total of 1,500 epochs using early stopping with patience parameter 10, learning rate of 5×10^{-3}, batch size of 100, and with the AdamW optimizer.

Unlike most graph neural network model which descriptors are based on atomic distance information, the ALIGNN[35] model incorporates bond angles which are important for distinguishing many atomic structures. This addition of bond angles gives the ALIGNN model better performance over others graph neural network model. The ALIGNN model was specifically trained and used to screen for low LTC structures. The ALIGNN model was trained on the same 10,158 elastic constants data obtained from the Jarvis-DFT database, with 80% of the data used for training and 20% for testing. Our ALIGNN model was trained for a total of 2,000 epochs, learning rate of 1×10^{-3}, batch size of 100, and with the AdamW

optimizer.

2.2 DFT calculations

For validation of mechanical properties of recommended structures by the deeperGATGNN, the DFT calculations are performed using the plane-wave basis projector augmented wave (PAW) method[43] within the Perdew-Burke-Ernzerhof exchange-correlation functional[44] as implemented in the VASP package[45–47]. The cutoff energy is set to 520 eV for the recommended crystal structures to calculate hardness. The energy and force criteria for the DFT calculation of elastic constants were 10^{-6} eV and 10^{-4} eV/Å, respectively. Parameters IBRION=6 (second derivatives and Hessian matrix calculation) and NFREE = 4 (number of ionic displacements in frozen phonon calculations) were used for computing elastic constants in VASP package. For k-points for electrons, we generally use the product of the number of k-points and the lattice parameter in that specific direction at least 50 Å. The phonon dispersions of selected structures were calculated by the finite displacement method using PHONOPY package[48] with the atomic forces for the harmonic second-order force constants calculated by VASP. The corresponding interatomic force constants were obtained using 3 × 3 × 3 supercells and with KPOINTS resolution of 4 × 4 × 4 for high precision self-consistent static DFT calculations. For DFT calculation of LTC, the second and third order interatomic force constants were fitted to at least 20 random displaced supercells for each structure by the compressive sensing lattice dynamics (CSLD) method[49], which extracts the IFC from Taylor-expanded interatomic forces in terms of atomic displacement via advanced compressive sensing techniques. The 3rd order interatomic force constants for all materials were truncated to the third nearest neighbors. The LTC calculation was solved by phonon Peierls Boltzmann transport equation (BTE) with the ShengBTE package[50]. The ngrid parameter, which is used for sampling the entire Brillouin zone (BZ), was chosen to be at least 16×16×16 for cubic structures, or equivalent numbers for noncubic structures, or the total number of scattering events on the order of 2 to 5×10^{8}, whichever is larger.

3. RESULTS AND DISCUSSION

In Fig. 1, we show the statistics of our training and prediction data. Fig. 1a, b shows the number of space group types in our training and prediction data. All 230 space groups categorized into triclinic, monoclinic, orthorhombic, tetragonal, trigonal, hexagonal, and cubic were included in our training and prediction data. For the training data, the majority space groups are tetragonal and cubic symmetries, while for the prediction data the distribution of all space groups is uniform. Note that Fig. 1b shows the log-scale of the space group counts in the prediction data. Fig. 1c, d shows the number of elements in the training and prediction data, respectively. Both our training and prediction data cover 87 elements across the periodic table, and the distribution of all elements is uniform for the training and prediction data. From Fig. 1, we can see that the samples seen during training are independently and identically distributed, and they are drawn from the same distribution as unseen samples. This will help us avoid the so-called dataset shift issue during training. Therefore, predictions made by the model should have a small uncertainty, as we will see later.

3.1 Bulk modulus

The bulk modulus describes the strain response of a body to hydrostatic stress involving change in volume without change in shape i.e., resistance to compression[51]. It is defined as the reciprocal of compressibility[52]. It can predict compression and indirectly indicate the types of chemical bonding within substance. The application of bulk modulus is not limited to optimization of mechanical performance of materials[53], but it could be employed in optimizing materials for low LTC application[54]. In our study we trained the deeperGATGNN model that can predict the bulk modulus of materials with R^2 0.9438 and mean absolute error (MAE) 7.94 GPa as shown in Fig. 2. We also see that

the distribution of bulk modulus is wide and uniform, i.e., from low values (just a few GPa) to high values up to ~400GPa. The deeperGATGNN model can capture the atomic features inherent in the atomic structures.

3.2 Shear modulus

The shear modulus describes material response to the shear deformation, and it involves change in shape without change in volume[51]. It is defined as the ratio of shear stress and shear strain. This mechanical property tells us how resistant a material is to shearing deformation. In our study we trained the deeperGATGNN model that can predict the shear modulus of materials with R^2 0.8675 and MAE 7.79GPa as shown in Fig. 3. In contrast to the bulk modulus, we notice that the distribution of the shear modulus is not uniform. Unlike bulk modulus, the shear modulus has biased distribution. The majority of structures have shear modulus less than 200GPa, while only several structures possess shear modulus higher than 200GPa and very few above 400GPa. Despite such highly biased data distribution, the deeperGATGNN model still correctly captures the bonding nature in the structures and yields a high R^2 score.

3.3 Young's modulus

The Young's modulus is a mechanical property that measures the tensile or compressive stiffness of a material when force is applied, and it is defined as the ratio of tensile stress to tensile strain[55]. It describes the yield strength of a material. In our study we trained the deeperGATGNN model that can predict the young's modulus of materials with R^2 0.8567 and mean absolute error 19.62GPa as shown in Fig. 4. The Young's modulus has an extremely wide range of distribution, i.e., from nearly zero to up to ~1,000GPa. Still, the deeperGATGNN model is successful in training and has a relatively high R^2 score in validation. It is worth noting that, for extremely high modulus, the prediction error could be higher, since there are very limited number of training data in that range and thus the model was not trained very well for those regions. Adding more data in the rare regions will significantly improve the quality of the model.

3.4 Poisson's ratio

Poisson's ratio measures how a material deforms under stress, and it is defined as the ratio of the lateral contraction to the elongation[56]. It is important because it allows materials to be chosen that suit the desired function. Materials with negative Poisson's ratio are of high importance because they improve mechanical properties[57] such as toughness, shear resistance, and they used in several applications such as in medicine, sports, automobile, and defense. In our study, we trained the deeperGATGNN model that can predict the Poisson's ratio of materials with R^2 0.5409 and mean absolute error 0.027 as shown in Fig. 5. It is worth noting that we do not have any negative Poisson's ratio materials in our training dataset. Therefore, as the usual trend of traditional machine learning models, it is highly expected that we will not be able to identify too many negative Poisson's ratio materials in the screening pool as well. Although the extrapolation ability is a common problem for most of machine learning models, new approaches have been developed recently to expand the trained models to unknown or unseen regions, such as the boundless objective-free exploration method[24]. Such approaches are promising for pushing the original material properties to the limit or beyond the current range.

3.5 Hardness

Hardness characterizes the property of a material to resist plastic deformation, therefore hardness is important from an engineering standpoint because resistance to wear generally increases with hardness. In our study, we trained the deeperGATGNN model that can predict hardness of materials with R^2 0.7581 and mean absolute error 1.66GPa as shown in Fig. 6a. Like shear modulus, the hardness distribution is

also highly non-uniform or biased. Most of the structures have hardness below 40GPa, while only several structures possess hardness above 40GPa, the so-called super hard materials. With the trained deeperGATGNN model, we predicted on 775,947 crystal structures from the OQMD, and we identify 20 structures with ultrahigh hardness (hardness exceeding 40GPa[23]) close to that of diamond, as shown in Table 1. We also list other relevant material information such as space group, bandgap in Table 1. We find that those super hard materials have quite different space groups or structural symmetry, meaning that ultrahard materials do not necessarily happen in some specific space groups. We also find that the bandgap is irrelevant to the hardness of a material, as we can see from Table 1 the 20 structures have large range of bandgaps. Fig. 6b shows the hardness of predicted structures and the validated DFT calculations for our 20 top ranked structures. Of the 20 top ranked structures, to the best of our knowledge, two structures, namely $B_2C_4N_2$ and C_6N_8, have not been reported in literature. The two new structures turned out again to be compositions of B-C-N elements, which follow the general trend of majority of the known ultrahigh hardness materials.

3.6 Data-driven insight to hardness

Here, we perform further study to deeply understand the bonding nature of the structures with ultrahigh hardness. In principle, the mechanical behavior of a material depends on its interatomic bonding, which can be traced backed to the spatial distribution of electron clouds. To analyze the mechanism for hardness, we establish a correlation between electron work function (EWF), which is the minimum energy required to move electrons inside a material at the Fermi level to its surface without kinetic energy[58], interatomic bonding, and hardness. Most known super hard materials like diamond have a strong covalent bonding[59], and previous studies have shown that the higher the EWF, the higher the hardness[59]. We also study the electron localization function (ELF) which is the measure of electron localization in atomic structures. The ELF in Fig. 7 reflects the probability of finding an electron in the structure and the local potential (LOCPOT) for the two super hard structures, namely $B_2C_4N_2$ (structure ID: 16166, hardness: ~76 GPa) and C_6N_8 (structure ID: 14925, hardness: ~52 GPa), that have never been published in literature to the best of our knowledge. Figs. 7a, b also shows the possibility of finding an electron and strong covalent bond existing between the elements of the material, which explains why the materials have high hardness. Figs. 7c, d also show the presence of strong covalent bonds between the atoms of the structures, which is a strong feature or indication for high hardness. Thus, all figures agree with the high hardness exhibited by all structures as confirmed by DFT calculations.

Figure 8 shows the phonon dispersion curves for the two structures that have not been reported in literature. We can see that both structures are thermodynamically stable since there are no negative frequencies found in the Brillouin zone. We also find that, the cutoff frequency in both structures is as high as 40 THz, which is consistent with the high modulus and light element (boron, carbon, and nitrogen) of both structures, because the speed of sound or group velocity of phonons is generally proportional to the square root of Young's modulus and inversely proportional to the square root of mass density ($v_s \sim \sqrt{E/\rho}$). We also noticed that the frequency of the acoustic phonon modes can go up to 10 to 15 THz, which is comparable to that for diamond, another material that has extremely high hardness. Again, this result is consistent with the previous DFT results of ultrahigh hardness where strong interatomic bonding is necessary.

3.7 Low lattice thermal conductivity prediction

Prediction of LTC is very important to material scientists and engineers since it has many applications ranging from thermal management to energy conversion. However, the accurate measurement or prediction of LTC is cumbersome. From the classical molecular dynamics to empirical models, prediction is efficient but less accurate, while prediction from full first-principles calculations like DFT is accurate

but less efficient. ML models help us in bridging the gap between accuracy and efficiency, but accurate training of an LTC ML model is also difficult due to unavailability of many high quality LTC data needed to train a good model. According to the kinetic theory of phonon transport[60] and using the single mode relaxation time approximation of the Boltzmann equation, the total thermal conductivity contributed by phonon modes can be expressed as

$$\kappa = \sum_i C_i(\boldsymbol{q}) v_i^2(\boldsymbol{q}) \tau_i(\boldsymbol{q}) \quad (3)$$

Where the summation is conducted to all phonon modes, C_i is the specific heat of a specific phonon mode represented by wave vector $\boldsymbol{q}$, v_i is the group velocity, and τ_i is the phonon relaxation time (lifetime). From Eq. (3) we know that, if the phonon group velocity is significantly reduced, the thermal conductivity is anticipated to be very low. Therefore, it is an intuitive idea to search low LTC materials by alternatively screening low group velocity materials. From physics law, we also know that the phonon group velocity can be roughly estimated as $v \propto \sqrt{E/\rho}$, where E is the Young's modulus characterizing the bonding strength and ρ is the mass density of the material. We finally choose bulk modulus for searching low LTC materials based on following reasons: (1) From our previous ML models' results, in particular comparing Figs. 2 and 4, the performance of deeperGATGNN model on bulk modulus is way higher than that on Young's modulus. Using a more accurate ML model for materials screening would lead to less uncertainty for the finally filtered-out structures. (2) The bulk modulus (B) is also directly correlated with the Young's modulus by $B = \frac{E}{3(1-2\nu)}$, where ν is the Poisson's ratio. Considering that the Poisson's ratio does not change too much among all structures tested herein, as has been treated as a constant in many previous studies for mechanics, the bulk modulus can be almost solely dependent on the Young's modulus. Therefore, we expect that there is a positive correlation between bulk modulus and LTC. It is worth noting that, we did a separate test by training a machine learning model (ALIGNN) on bulk modulus (B) only, the ratio of bulk modulus to density (B/ρ), and the square root of the ratio between bulk modulus and density ($\sqrt{B/\rho}$). We find that there is no significant difference among all three models, as shown in Figure S1 in Supplementary Information. We also trained ALIGNN on Young's modulus (E), the ratio of Young's modulus to density (E/ρ), and the square root of Young's modulus to density ($\sqrt{E/\rho}$). For all properties used, the bulk modulus has the best performance (the highest R^2 score) as shown in Figure S1 and S2 in Supplementary Information. Therefore, we only use the bulk modulus for our screening.

We first trained a high quality ALIGNN model for bulk modulus using the same high quality DFT data as deeperGATGNN. We did a further prediction of bulk modulus and comparison using ALIGNN, orbital graph convolutional neural network (OGCNN), deeperGATGNN, and crystal graph convolutional neural network (CGCNN). Again, the ALIGNN model was the best performing model among all four graph neural networks trained and tested (see Figure S2 in the Supplementary Information for testing results). Fig. 9a shows our trained ALIGNN model for the test result of bulk modulus on 20% of our 10,158 elastic constants training data. The ALIGNN model predicts the bulk modulus of materials with R^2 value of 0.98 and mean absolute error (MAE) of 5.354 GPa. This shows that the ALIGNN model has much higher performance than the deeperGATGNN model as shown in Fig. 2. The ALIGNN model performs very well because it incorporates both bond length and bond angles information in the descriptors, which is important factors contributing to mechanical properties of crystalline materials and play dominant roles in determining harmonic interatomic force constants.

We then use the trained ALIGNN model to predict the bulk modulus of all 775,947 structures taken from the OQMD database. After model prediction, we sort the predicted bulk modulus from low to high and get the recommended potential materials with low LTC, corresponding to low bulk modulus. We verify the LTC of 338 recommended structures as seen in Fig. 9b. From Fig. 9b we can see that, overall, the LTC

has a strong positive correlation with bulk modulus, as expected earlier by us, which also validated our previous hypothesis. Moreover, the structures with bulk modulus below 130 GPa have LTC value in the range of 0.1 – 10 W/mK and in total 273 structures possess LTC below 10 W/mK. Information about all recommended 338 structures, including OQMD structure ID, space group number, number of atoms in the unit cell, corresponding LTC values by full DFT calculations, are given in Table S1 in the Supplementary Information. With this result, we can conclude that bulk modulus is an effective and accurate index to serve as an indicator to screen and recommend materials with low or high LTC when there is no sufficient high quality LTC data for training a ML model. With our high quality DFT LTC data, we believe it will benefit other researchers for future training high fidelity LTC ML models.

4. CONCLUSIONS

In summary, we build a scalable global attention graph neural network model to screen extreme mechanical properties (bulk modulus, shear modulus, Young's modulus, Poisson's ratio, and hardness) of materials, which is trained on elastic properties of 10,158 materials. We deployed the trained hardness model to predict 775,947 inorganic crystal structures from the open quantum materials database to search super hard materials. We finally identified 20 structures with ultrahigh hardness. Among these predictions, two structures, namely $B_2C_4N_2$ (structure ID: 16166, space group number: 17) and C_6N_8 (structure ID: 14925, space group number: 220) have not been reported in previous studies and possess ultrahigh hardness of 76 GPa and 52 GPa, respectively. These hardness results were validated by high precision DFT calculations and deep insight into the ultrahigh hardness was understood from electronic level. We also trained a high quality atomistic line graph neural network model for bulk modulus and applied it to predict bulk modulus of 775,947 structures, from which we recommend potential structures with low lattice thermal conductivity, which is a critical physical property for rational design of high performance thermoelectric energy conversion systems and thermal insulation structures. We continue to verify the lattice thermal conductivity of 338 predicted structures by conducting first principles calculations and solving the phonon Peierls Boltzmann transport equation. Considering the total number of first principles calculations is only 0.04% of all 775,947 structures that have been screened, the approach of combining machine learning and first principles is very promising for accelerating discovery of novel energy materials with high efficiency and accuracy, such as energy efficiency electronics.

Authors' contributions

Performed data acquisition, model training, data analysis and interpretation: Joshua Ojih, Alejandro Rodriguez
Conception and design of the study: Ming Hu
Performed data analysis and interpretation: Ming Hu, Jianjun Hu
Funding acquisition: Ming Hu, Jianjun Hu

Availability of data and materials

The data that support the findings of this study are available from the corresponding author upon reasonable request.

Acknowledgements

This work was supported by the NSF (award number 2110033), NASA SC Space Grant Consortium REAP Program (Award No.: 521383-RP-SC004), SC EPSCoR/IDeA Program under NSF OIA-1655740 (23-GC01) and ASPIRE grant from the Office of the Vice President for Research at the University of South Carolina (project 80005046).

Conflicts of interest

All authors declared that there are no conflicts of interest.

References

[1] Stoll, A., and Benner, P., 2021, "Machine Learning for Material Characterization with an Application for Predicting Mechanical Properties," GAMM Mitteilungen, **44**(1), pp. 1–21.

[2] De Jong, M., Chen, W., Angsten, T., Jain, A., Notestine, R., Gamst, A., Sluiter, M., Ande, C. K., Van Der Zwaag, S., Plata, J. J., Toher, C., Curtarolo, S., Ceder, G., Persson, K. A., and Asta, M., 2015, "Charting the Complete Elastic Properties of Inorganic Crystalline Compounds," Sci. Data, **2**, pp. 1–13.

[3] Niu, H., Chen, X. Q., Liu, P., Xing, W., Cheng, X., Li, D., and Li, Y., 2012, "Extra-Electron Induced Covalent Strengthening and Generalization of Intrinsic Ductile-to-Brittle Criterion," Sci. Rep., **2**, pp. 1–6.

[4] Wu, S., Yan, T., Kuai, Z., and Pan, W., 2020, "Thermal Conductivity Enhancement on Phase Change Materials for Thermal Energy Storage: A Review," Energy Storage Mater., **25**(September 2019), pp. 251–295.

[5] Francoeur, M., Vaillon, R., and Meng, M. P., 2011, "Thermal Impacts on the Performance of Nanoscale-Gap Thermophotovoltaic Power Generators," IEEE Trans. Energy Convers., **26**(2), pp. 686–698.

[6] Zhou, Y., Xiong, S., Zhang, X., Volz, S., and Hu, M., 2018, "Thermal Transport Crossover from Crystalline to Partial-Crystalline Partial-Liquid State," Nat. Commun., **9**(1), pp. 1–8.

[7] Wang, H., Qin, G., Yang, J., Qin, Z., Yao, Y., Wang, Q., and Hu, M., 2019, "First-Principles Study of Electronic, Optical and Thermal Transport Properties of Group III-VI Monolayer MX (M = Ga, In; X = S, Se)," J. Appl. Phys., **125**(24).

[8] Wang, H., Qin, G., Li, G., Wang, Q., and Hu, M., 2017, "Low Thermal Conductivity of Monolayer ZnO and Its Anomalous Temperature Dependence," Phys. Chem. Chem. Phys., **19**(20), pp. 12882–12889.

[9] Tang, D. S., Qin, G. Z., Hu, M., and Cao, B. Y., 2020, "Thermal Transport Properties of GaN with Biaxial Strain and Electron-Phonon Coupling," J. Appl. Phys., **127**(3).

[10] Qin, G., and Hu, M., 2018, "Accelerating Evaluation of Converged Lattice Thermal Conductivity," npj Comput. Mater., **4**(1).

[11] Agrawal, A., and Choudhary, A., 2016, "Perspective: Materials Informatics and Big Data: Realization of the 'Fourth Paradigm' of Science in Materials Science," APL Mater., **4**(5).

[12] Noh, J., Gu, G. H., Kim, S., and Jung, Y., 2020, "Uncertainty-Quantified Hybrid Machine Learning/Density Functional Theory High Throughput Screening Method for Crystals," J. Chem. Inf. Model., **60**(4), pp. 1996–2003.

[13] MacKerell, A. D., Bashford, D., Bellott, M., Dunbrack, R. L., Evanseck, J. D., Field, M. J., Fischer, S., Gao, J., Guo, H., Ha, S., Joseph-McCarthy, D., Kuchnir, L., Kuczera, K., Lau, F. T. K., Mattos, C., Michnick, S., Ngo, T., Nguyen, D. T., Prodhom, B., Reiher, W. E., Roux, B., Schlenkrich, M., Smith, J. C., Stote, R., Straub, J., Watanabe, M., Wiórkiewicz-Kuczera, J., Yin, D., and Karplus, M., 1998, "All-Atom Empirical Potential for Molecular Modeling and Dynamics Studies of Proteins," J. Phys. Chem. B, **102**(18), pp. 3586–3616.

[14] Schmidt, J., Marques, M. R. G., Botti, S., and Marques, M. A. L., 2019, "Recent Advances and Applications of Machine Learning in Solid-State Materials Science," npj Comput. Mater., **5**(1).

[15] Louis, S. Y., Zhao, Y., Nasiri, A., Wang, X., Song, Y., Liu, F., and Hu, J., 2020, "Graph Convolutional Neural Networks with Global Attention for Improved Materials Property Prediction," Phys. Chem. Chem. Phys., **22**(32), pp. 18141–18148.

[16] Agrawal, A., and Choudhary, A., 2019, "Deep Materials Informatics: Applications of Deep Learning in Materials Science," MRS Commun., **9**(3), pp. 779–792.

[17] Gonzalez, T. F., 2007, "Handbook of Approximation Algorithms and Metaheuristics," Handb. Approx. Algorithms Metaheuristics, pp. 1–1432.

[18] Ojih, J., Onyekpe, U., Rodriguez, A., Hu, J., Peng, C., and Hu, M., 2022, "Machine Learning Accelerated Discovery of Promising Thermal Energy Storage Materials with High Heat Capacity."

[19] Rodriguez, A., Liu, Y., and Hu, M., 2020, "Spatial Density Neural Network Force Fields with First-Principles Level Accuracy and Application to Thermal Transport," Phys. Rev. B, **102**(3), p. 35203.
[20] Qin, G., Wei, Y., Yu, L., Xu, J., Ojih, J., Rodriguez, A. D., Wang, H., Qin, Z., and Hu, M., 2023, "Predicting Lattice Thermal Conductivity from Fundamental Material Properties Using Machine Learning Techniques," J. Mater. Chem. A, pp. 5801–5810.
[21] Li, S., Dan, Y., Li, X., Hu, T., Dong, R., Cao, Z., and Hu, J., 2020, "Critical Temperature Prediction of Superconductors Based on Atomic Vectors and Deep Learning," Symmetry (Basel)., **12**(2).
[22] Mansouri Tehrani, A., Oliynyk, A. O., Parry, M., Rizvi, Z., Couper, S., Lin, F., Miyagi, L., Sparks, T. D., and Brgoch, J., 2018, "Machine Learning Directed Search for Ultraincompressible, Superhard Materials," J. Am. Chem. Soc., **140**(31), pp. 9844–9853.
[23] Al-Fahdi, M., Ouyang, T., and Hu, M., 2021, "High-Throughput Computation of Novel Ternary B-C-N Structures and Carbon Allotropes with Electronic-Level Insights into Superhard Materials from Machine Learning," J. Mater. Chem. A, **9**(48), pp. 27596–27614.
[24] Ojih, J., Al-fahdi, M., Rodriguez, A. D., and Choudhary, K., "Efficiently Searching Extreme Mechanical Properties via Boundless Objective-Free Exploration and Minimal First-Principles Calculations," pp. 1–12.
[25] Wen, Y., Wang, L., Liu, H., and Song, L., 2017, "Properties of B19 TiAl," pp. 1–11.
[26] Li, H., Gutierrez, L., Toda, H., Kuwazuru, O., Liu, W., Hangai, Y., Kobayashi, M., and Batres, R., 2016, "Identification of Material Properties Using Nanoindentation and Surrogate Modeling," Int. J. Solids Struct., **81**, pp. 151–159.
[27] Fan, J., Han, F., and Liu, H., 2014, "Challenges of Big Data Analysis," Natl. Sci. Rev., **1**(2), pp. 293–314.
[28] Keith, J. A., Vassilev-Galindo, V., Cheng, B., Chmiela, S., Gastegger, M., Müller, K. R., and Tkatchenko, A., 2021, "Combining Machine Learning and Computational Chemistry for Predictive Insights into Chemical Systems," Chem. Rev., **121**(16), pp. 9816–9872.
[29] Seko, A., Maekawa, T., Tsuda, K., and Tanaka, I., 2014, "Machine Learning with Systematic Density-Functional Theory Calculations: Application to Melting Temperatures of Single- and Binary-Component Solids," Phys. Rev. B - Condens. Matter Mater. Phys., **89**(5), pp. 1–9.
[30] Pun, G. P. P., Batra, R., Ramprasad, R., and Mishin, Y., 2019, "Physically Informed Artificial Neural Networks for Atomistic Modeling of Materials," Nat. Commun., **10**(1), pp. 1–10.
[31] Lapuschkin, S., Wäldchen, S., Binder, A., Montavon, G., Samek, W., and Müller, K. R., 2019, "Unmasking Clever Hans Predictors and Assessing What Machines Really Learn," Nat. Commun., **10**(1), pp. 1–8.
[32] Ojih, J., 2021, "Searching Extreme Mechanical Properties Using Active Machine Learning and Density Functional Theory."
[33] Omee, S. S., Louis, S.-Y., Fu, N., Wei, L., Dey, S., Dong, R., Li, Q., and Hu, J., 2021, "Scalable Deeper Graph Neural Networks for High-Performance Materials Property Prediction," Patterns, **3**(5), p. 100491.
[34] Xie, T., and Grossman, J. C., 2018, "Crystal Graph Convolutional Neural Networks for an Accurate and Interpretable Prediction of Material Properties," Phys. Rev. Lett., **120**(14), p. 145301.
[35] Choudhary, K., and DeCost, B., 2021, "Atomistic Line Graph Neural Network for Improved Materials Property Predictions," npj Comput. Mater., **7**(1), pp. 1–8.
[36] Saal, J. E., Kirklin, S., Aykol, M., Meredig, B., and Wolverton, C., 2013, "Materials Design and Discovery with High-Throughput Density Functional Theory: The Open Quantum Materials Database (OQMD)," Jom, **65**(11), pp. 1501–1509.
[37] Kirklin, S., Saal, J. E., Meredig, B., Thompson, A., Doak, J. W., Aykol, M., Rühl, S., and Wolverton, C., 2015, "The Open Quantum Materials Database (OQMD): Assessing the Accuracy of DFT Formation Energies," npj Comput. Mater., **1**(October).

[38] Choudhary, K., Garrity, K. F., Reid, A. C. E., DeCost, B., Biacchi, A. J., Hight Walker, A. R., Trautt, Z., Hattrick-Simpers, J., Kusne, A. G., Centrone, A., Davydov, A., Jiang, J., Pachter, R., Cheon, G., Reed, E., Agrawal, A., Qian, X., Sharma, V., Zhuang, H., Kalinin, S. V., Sumpter, B. G., Pilania, G., Acar, P., Mandal, S., Haule, K., Vanderbilt, D., Rabe, K., and Tavazza, F., 2020, "The Joint Automated Repository for Various Integrated Simulations (JARVIS) for Data-Driven Materials Design," npj Comput. Mater., **6**(1).

[39] Choudhary, K., Cheon, G., Reed, E., and Tavazza, F., 2018, "Elastic Properties of Bulk and Low-Dimensional Materials Using van Der Waals Density Functional," Phys. Rev. B, **98**(1), pp. 1–12.

[40] Hu, J., Stefanov, S., Song, Y., Omee, S. S., Louis, S. Y., Siriwardane, E. M. D., Zhao, Y., and Wei, L., 2022, "MaterialsAtlas.Org: A Materials Informatics Web App Platform for Materials Discovery and Survey of State-of-the-Art," npj Comput. Mater., **8**(1), pp. 1–12.

[41] Wang, X., Ji, H., Cui, P., Yu, P., Shi, C., Wang, B., and Ye, Y., 2019, "Heterogeneous Graph Attention Network," Web Conf. 2019 - Proc. World Wide Web Conf. WWW 2019, pp. 2022–2032.

[42] Veličković, P., Casanova, A., Liò, P., Cucurull, G., Romero, A., and Bengio, Y., 2018, "Graph Attention Networks," 6th Int. Conf. Learn. Represent. ICLR 2018 - Conf. Track Proc., pp. 1–12.

[43] Blöchl, P. E., 1994, "Projector Augmented-Wave Method," Phys. Rev. B, **50**(24), pp. 17953–17979.

[44] Perdew, J. P., Burke, K., and Ernzerhof, M., 1996, "Generalized Gradient Approximation Made Simple," Phys. Rev. Lett., **77**(18), pp. 3865–3868.

[45] Kresse, G., and Hafner, J., 1993, "Ab Initio Molecular Dynamics for Liquid Metals," Phys. Rev. B, **47**(1), pp. 558–561.

[46] Joubert, D., 1999, "From Ultrasoft Pseudopotentials to the Projector Augmented-Wave Method," Phys. Rev. B - Condens. Matter Mater. Phys., **59**(3), pp. 1758–1775.

[47] Vargas-Hernández, R. A., 2020, "Bayesian Optimization for Calibrating and Selecting Hybrid-Density Functional Models," J. Phys. Chem. A, **124**(20), pp. 4053–4061.

[48] Togo, A., and Tanaka, I., 2015, "First Principles Phonon Calculations in Materials Science," Scr. Mater., **108**, pp. 1–5.

[49] Zhou, F., Nielson, W., Xia, Y., and Ozoliņš, V., 2019, "Compressive Sensing Lattice Dynamics. I. General Formalism," Phys. Rev. B, **100**(18), pp. 1–15.

[50] Li, W., Carrete, J., Katcho, N. A., and Mingo, N., 2014, "ShengBTE: A Solver of the Boltzmann Transport Equation for Phonons," Comput. Phys. Commun., **185**(6), pp. 1747–1758.

[51] Phani, K. K., and Sanyal, D., 2008, "The Relations between the Shear Modulus, the Bulk Modulus and Young's Modulus for Porous Isotropic Ceramic Materials," Mater. Sci. Eng. A, **490**(1–2), pp. 305–312.

[52] Mezouar, R., Bioud, N., and Benmakhlouf, A., 2022, "Correlation Trend between the Bulk Modulus , Micro Hardness and the Lattice Parameter of III-V Semiconductors," (April), pp. 8–11.

[53] Furmanchuk, A., Agrawal, A., and Choudhary, A., 2016, "Predictive Analytics for Crystalline Materials: Bulk Modulus," RSC Adv., **6**(97), pp. 95246–95251.

[54] Chen, W., Pöhls, J. H., Hautier, G., Broberg, D., Bajaj, S., Aydemir, U., Gibbs, Z. M., Zhu, H., Asta, M., Snyder, G. J., Meredig, B., White, M. A., Persson, K., and Jain, A., 2016, "Understanding Thermoelectric Properties from High-Throughput Calculations: Trends, Insights, and Comparisons with Experiment," J. Mater. Chem. C, **4**(20), pp. 4414–4426.

[55] Williams, H., 2022, "Measuring Young's Modulus with a Tensile Tester," Phys. Educ., **57**(2), pp. 4–8.

[56] Mott, P. H., Dorgan, J. R., and Roland, C. M., 2008, "The Bulk Modulus and Poisson's Ratio of 'Incompressible' Materials," J. Sound Vib., **312**(4–5), pp. 572–575.

[57] Qin, G., "Negative Poisson ' s Ratio in Two-Dimensional Honeycomb Structures," npj Comput. Mater., pp. 1–6.

[58] Density, C., 1970, "1970 Theory," **1**(12).

[59] Hua, G., and Li, D., 2012, "The Correlation between the Electron Work Function and Yield

Strength of Metals," Phys. Status Solidi Basic Res., **249**(8), pp. 1517–1520.

[60] Hu, M., and Poulikakos, D., 2012, "Si/Ge Superlattice Nanowires with Ultralow Thermal Conductivity," Nano Lett., **12**(11), pp. 5487–5494.

Table1. Structures identified by deeperGATGNN with corresponding material information and ultrahigh hardness validated by DFT calculations.

Material ID	Formula	Space Group	Bandgap	deeperGATGNN Prediction (GPa)	DFT Calculation (GPa)
637352	C_{16}	12	3.731	93.06	79.74
16166	$B_2C_4N_2$	17	2.374	76.02	75.67
16167	BC_2N	25	1.878	75.36	74.23
22418	BC_7	115	0	66.04	71.78
22421	BC_7	25	0	79.83	67.00
21183	B_2C_{10}	119	0	74.32	66.49
7494	B_2N_2	186	5.411	65.14	64.84
22419	BC_7	156	0	73.69	62.84
22422	B_3C_{21}	160	0	74.49	57.56
1214685	B_8	64	0	74.47	55.64
21185	BC_5	156	0	63.18	54.55
14925	C_6N_8	220	2.995	60.23	52.17
21186	B_2C_{10}	2	0	78.31	51.70
1106039	B_4N_4	225	1.557	50.92	46.98
22420	BC_7	215	0	86.77	59.24
1218562	B_4N_4	216	4.795	51.28	64.10
686735	C_8	227	4.37	97.80	94.37
599492	C_{16}	194	4.508	98.21	94.72
599493	C_{30}	166	4.622	92.64	94.99
610558	C_{16}	206	2.609	100.35	105.20

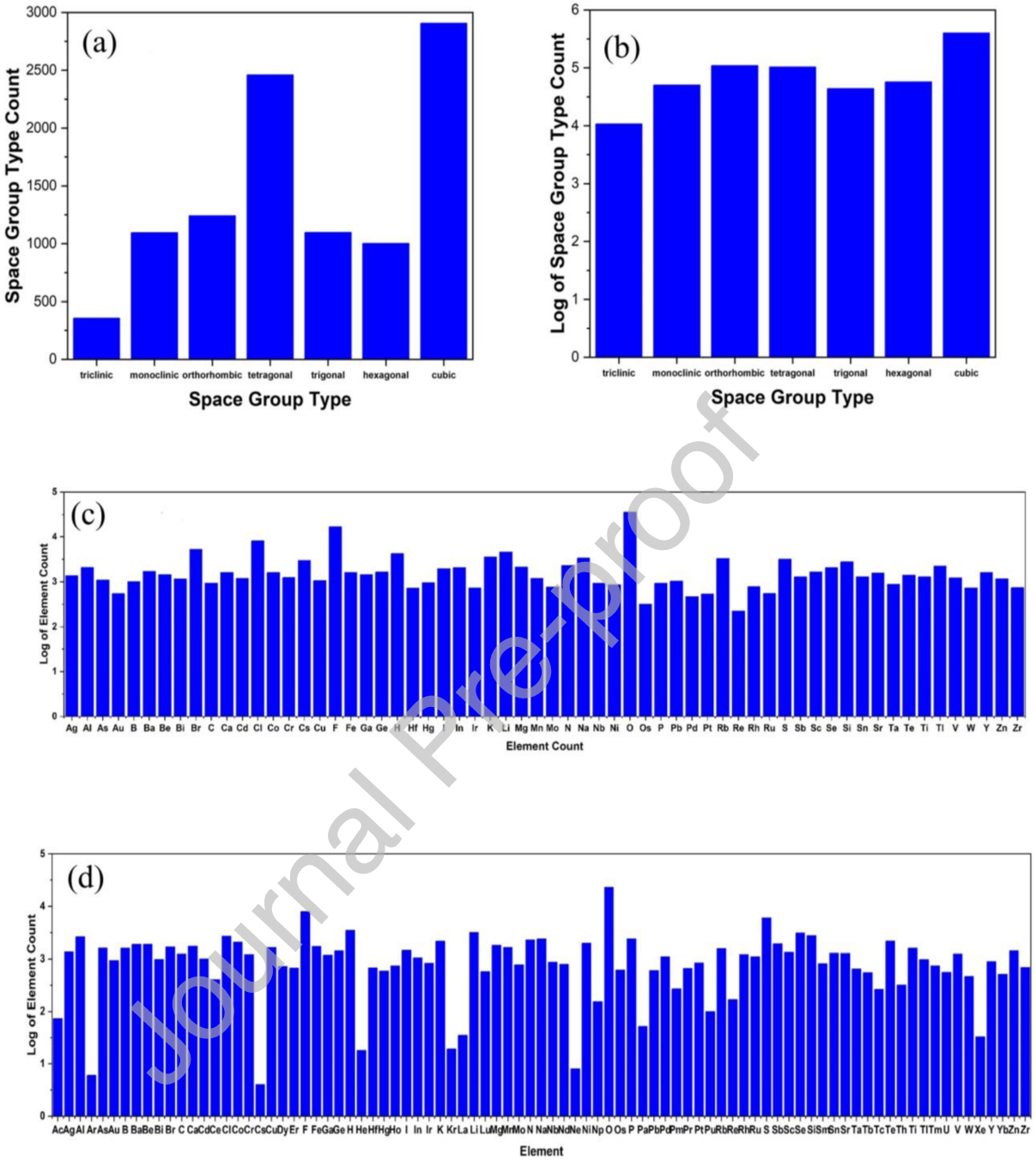

Figure 1. Statistics (structural symmetries and element distribution) for 10,158 training data and 775,947 prediction data. (a, b) shows the space group type for training and predicting data, respectively. (c, d) shows the element distribution for training and predicting data, respectively.

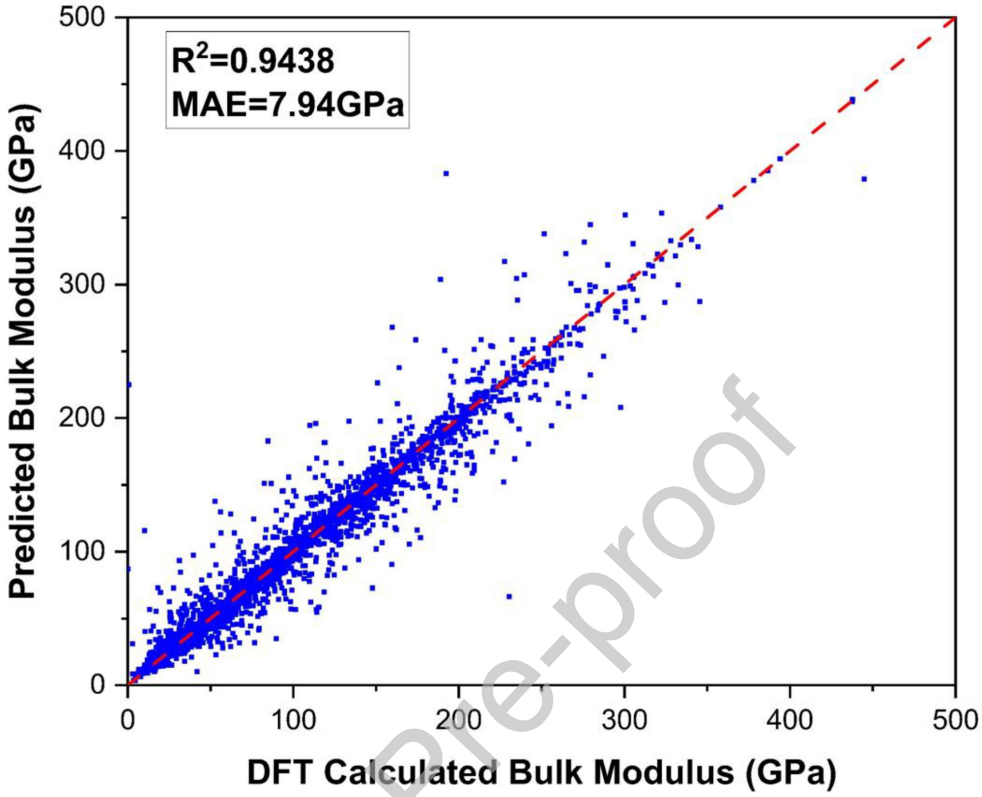

Figure 2. Testing result of the deeperGATGNN model for bulk modulus of 3,047 structures.

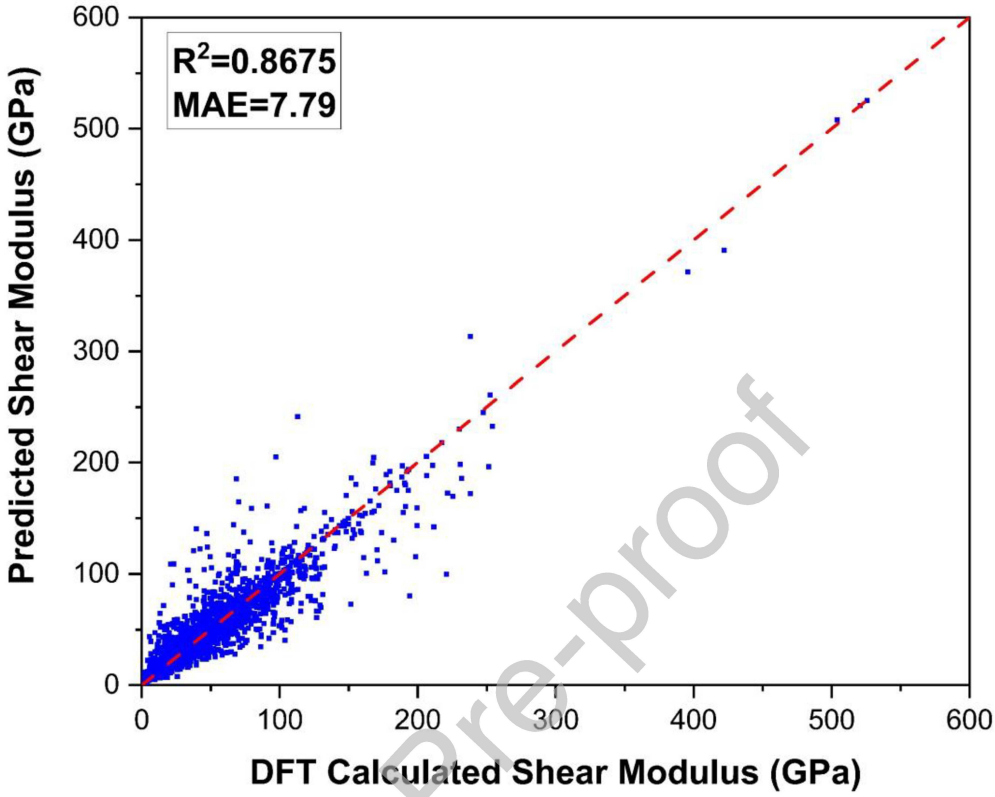

Figure 3. Testing result of the deeperGATGNN model for shear modulus of 3,047 structures.

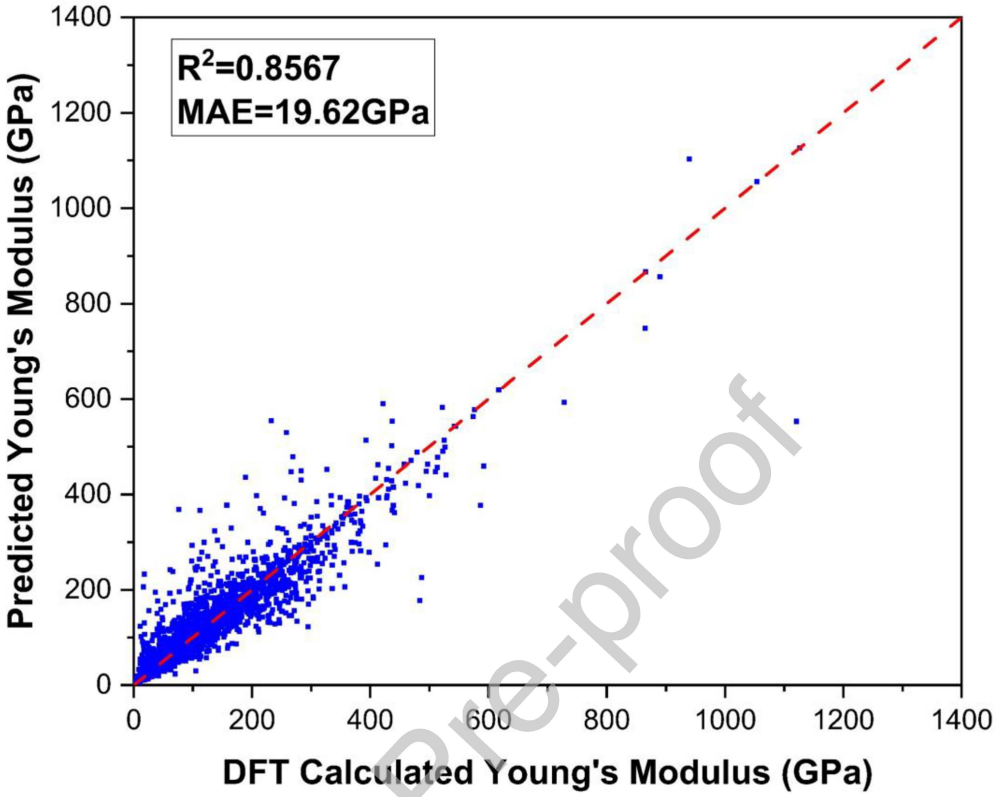

Figure 4. Testing result of the deeperGATGNN model for Young's modulus of 3,047 structures.

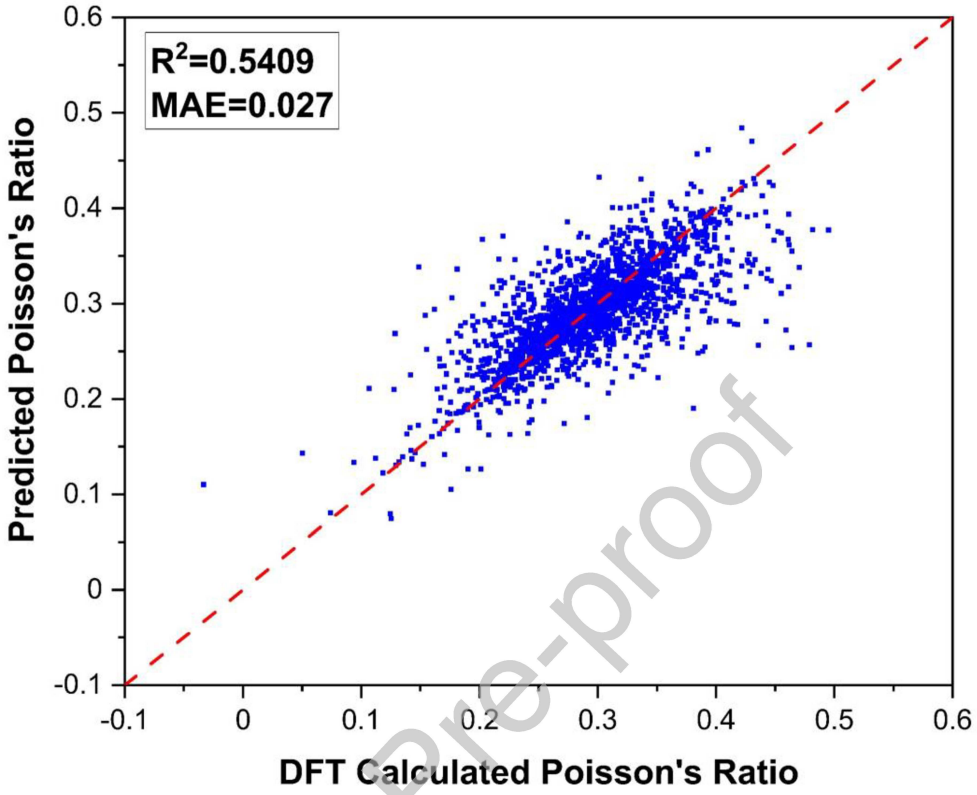

Figure 5. Testing result of the deeperGATGNN model for Poisson's ratio of 3,047 structures.

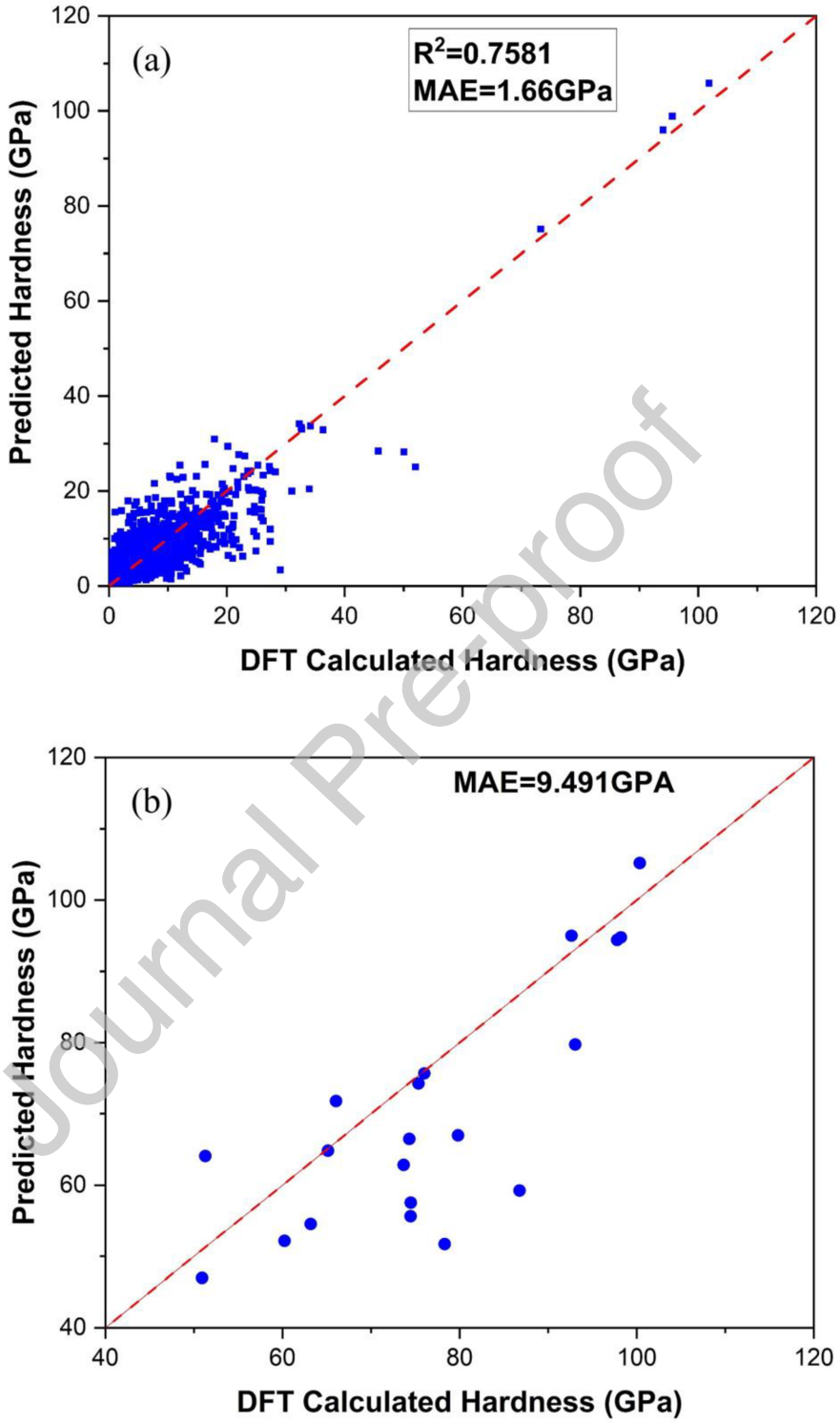

Figure 6. (a) Testing result of the deeperGATGNN model for hardness of 3,047 structures. (b) Comparison of deeperGATGNN prediction and DFT results for 20 recommended ultrahigh hardness structures.

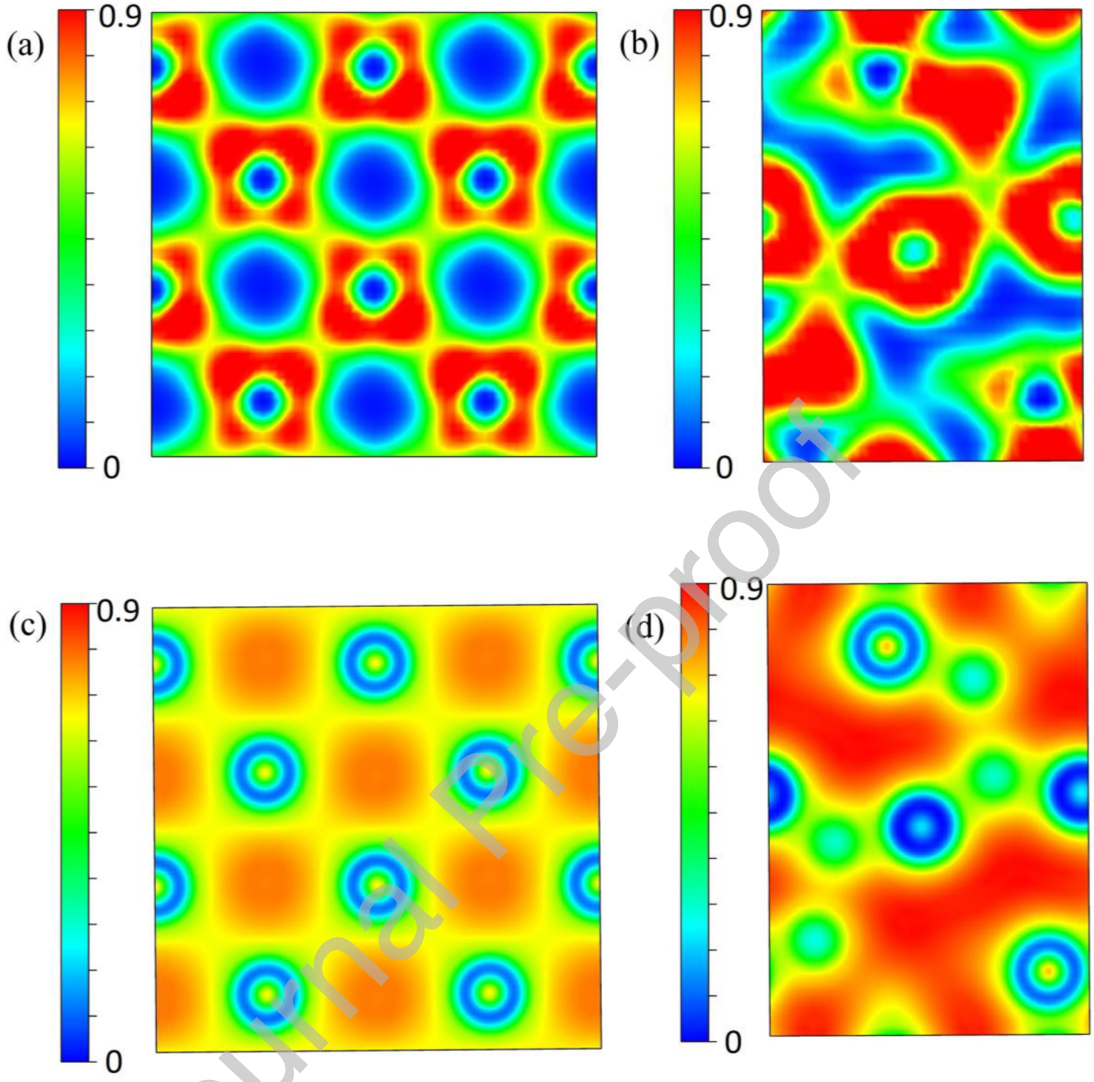

Figure 7. The electron localization function (ELF) (a, b) and local potential (LOCPOT) (c, d) of two identified ultrahard structures $Be_2C_4N_2$ (OQMD structure ID: 16166) (left panel) and C_6N_8 (OQMD structure ID: 14925) (right panel). Strong covalent bonding exists in both structures.

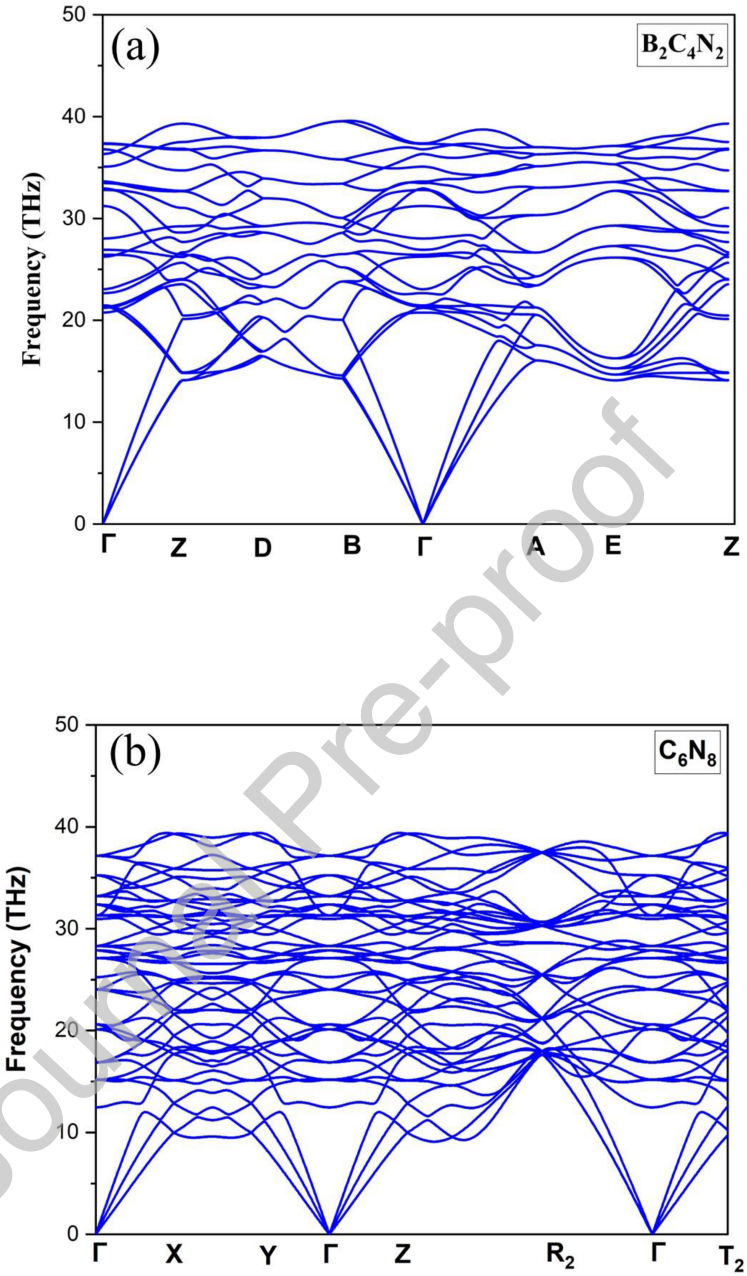

Fig. 8. Phonon dispersions of two identified ultrahard structures (a) $B_2C_4N_2$ and (b) C_6N_8 along high symmetry paths in the Brillouin zone. There is no negative frequency in phonon dispersions, indicating these structures are thermodynamically stable.

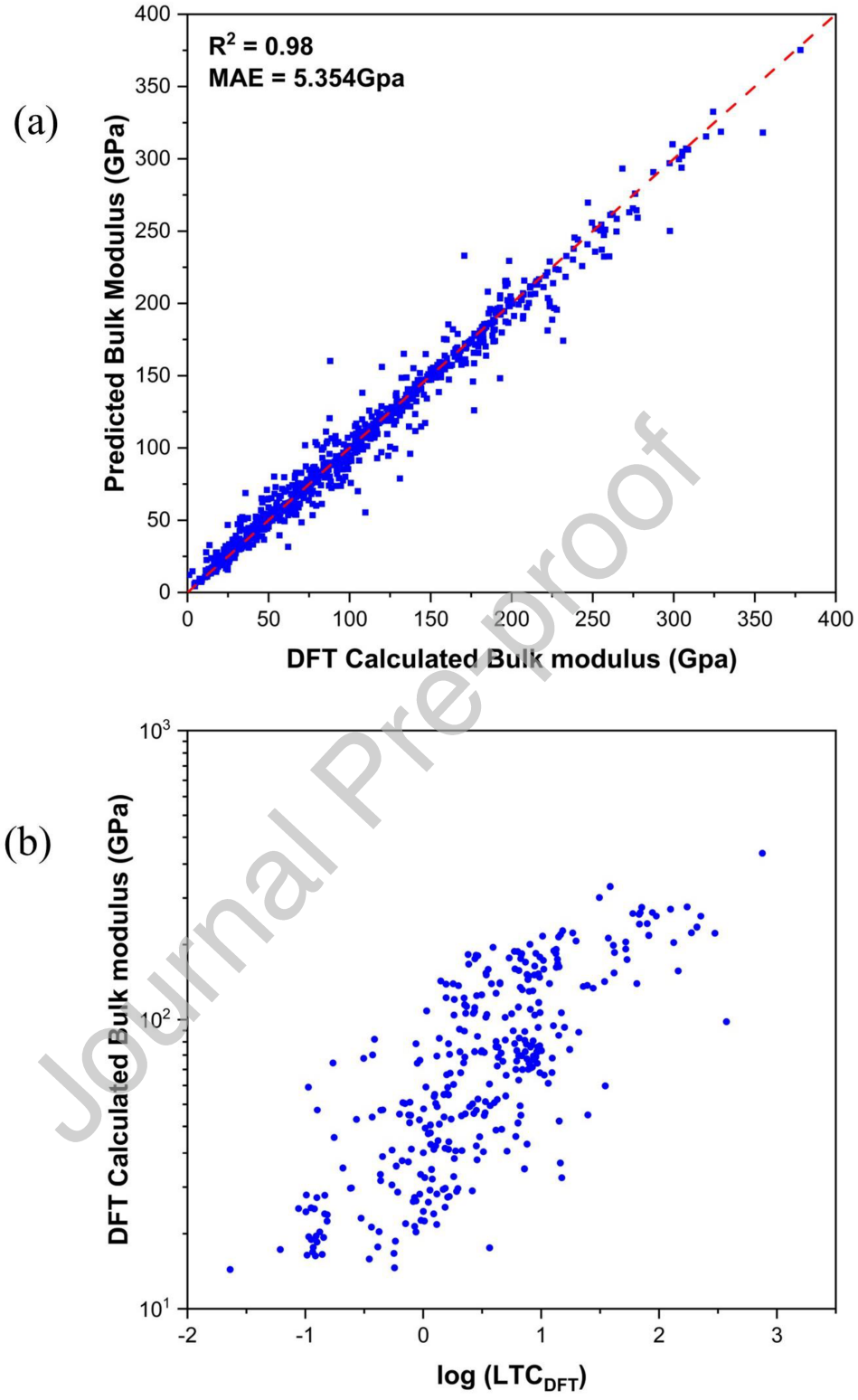

Figure 9. Testing result of the ALIGNN model for bulk modulus of 2,032 structures. (b) Correlation between bulk modulus and lattice thermal conductivity (LTC) for 338 recommended structures.

Declaration of Interests

All authors declared that there are no conflicts of interest.

Graphical Abstract